GFDL's CM2 Global Coupled Climate Models. Part IV: Idealized Climate Response

R. J. STOUFFER,* A. J. BROCCOLI,+ T. L. DELWORTH,* K. W. DIXON,* R. GUDGEL,* I. HELD,* R. HEMLER,* T. KNUTSON,* HYUN-CHUL LEE,#,& M. D. SCHWARZKOPF,* B. SODEN,@,** M. J. SPELMAN,* M. WINTON,* AND FANRONG ZENG#,&

*National Oceanic and Atmospheric Administration/Geophysical Fluid Dynamics Laboratory, Princeton University, Princeton, New Jersey

+ Department of Environmental Sciences, Rutgers–The State University of New Jersey, New Brunswick, New Jersey

RS Information Services, Inc., McLean, Virginia

@ University of Miami, Miami, Florida, and National Oceanic and Atmospheric Administration/Geophysical Fluid Dynamics Laboratory, Princeton University, Princeton, New Jersey

(Manuscript received 10 December 2004, in final form 27 June 2005)

ABSTRACT

The climate response to idealized changes in the atmospheric CO_2 concentration by the new GFDL climate model (CM2) is documented. This new model is very different from earlier GFDL models in its parameterizations of subgrid-scale physical processes, numerical algorithms, and resolution. The model was constructed to be useful for both seasonal-to-interannual predictions and climate change research. Unlike previous versions of the global coupled GFDL climate models, CM2 does not use flux adjustments to maintain a stable control climate. Results from two model versions, Climate Model versions 2.0 (CM2.0) and 2.1 (CM2.1), are presented.

Two atmosphere–mixed layer ocean or slab models, Slab Model versions 2.0 (SM2.0) and 2.1 (SM2.1), are constructed corresponding to CM2.0 and CM2.1. Using the SM2 models to estimate the climate sensitivity, it is found that the equilibrium globally averaged surface air temperature increases 2.9 (SM2.0) and 3.4 K (SM2.1) for a doubling of the atmospheric CO_2 concentration. When forced by a 1% per year CO_2 increase, the surface air temperature difference around the time of CO_2 doubling [transient climate response (TCR)] is about 1.6 K for both coupled model versions (CM2.0 and CM2.1). The simulated warming is near the median of the responses documented for the climate models used in the 2001 Intergovernmental Panel on Climate Change (IPCC) Working Group I Third Assessment Report (TAR).

The thermohaline circulation (THC) weakened in response to increasing atmospheric CO_2. By the time of CO_2 doubling, the weakening in CM2.1 is larger than that found in CM2.0: 7 and 4 Sv (1 Sv $\equiv 10^6$ m^3 s^{-1}), respectively. However, the THC in the control integration of CM2.1 is stronger than in CM2.0, so that the percentage change in the THC between the two versions is more similar. The average THC change for the models presented in the TAR is about 3 or 4 Sv; however, the range across the model results is very large, varying from a slight increase (+2 Sv) to a large decrease (−10 Sv).

1. Introduction

This paper documents the response of the newly developed global coupled climate models (CM2) to idealized radiative forcing changes. The CM2 models have been developed at the Geophysical Fluid Dynamics Laboratory (GFDL) in Princeton, New Jersey, and are intended to simulate the climate system over a wide range of time scales, from the diurnal cycle through multicentury climate change. The coupled model consists of newly developed atmosphere, ocean, land, and sea ice components.

The CM2 models use very different numerical algorithms and subgrid-scale physical parameterizations relative to the older R15 and R30 GFDL climate models (e.g., Manabe et al. 1991; Delworth et al. 2002) and the older GFDL seasonal-to-interannual (SI) forecast model (Rosati et al. 1997). The coupling of the new

& Current affiliation: National Oceanic and Atmospheric Administration/Geophysical Fluid Dynamics Laboratory, Princeton University, Princeton, New Jersey.

** Current affiliation: University of Miami, Miami, Florida.

Corresponding author address: Dr. Ronald J. Stouffer, National Oceanic and Atmospheric Administration/Geophysical Fluid Dynamics Laboratory, Princeton University, Forrestal Campus, U.S. Route 1, P.O. Box 308, Princeton, NJ 08542.
E-mail: Ronald.Stouffer@noaa.gov

CM2 physical climate model to a biogeochemical component model is under way.

The model development effort is accomplished using the new coding framework called the Flexible Modeling System (FMS, http://www.gfdl.noaa.gov/~fms) that was also developed at GFDL. This new coding paradigm seeks to hide many of the computer science issues from the physical scientists working on the coupled model code.

From the beginning of the effort, the goal was to build a coupled climate model that did not require the use of flux adjustments (Manabe and Stouffer 1988; Sausen et al. 1988) to maintain a stable control climate. Delworth et al. (2006, hereafter Part I) and Gnanadesikan et al. (2006, hereafter Part II) of this four-part set of papers describe the coupled and ocean component model performance in this new model, respectively. The reader is referred to those papers for more details on the comparison of the control simulations to the observed climate.

A second goal of the coupled model development effort was to build a climate model well suited for performing both decadal-to-centennial (DecCen) timescale investigations and seasonal-to-interannual (SI) forecasts and research. Wittenberg et al. (2006, hereafter Part III) evaluates the El Niño–Southern Oscillation (ENSO) in the multicentury control integrations.

The purpose of this paper is to document the response of the new climate models to an idealized change in the radiative forcing. For the coupled model, this idealized forcing is accomplished by increasing the atmospheric CO_2 concentration at a rate of 1% per year (compounded) to doubling. The climate sensitivity is evaluated using atmosphere–mixed layer or slab ocean models to a doubling of the atmospheric CO_2 concentration. The documentation presented here consists of only a general overview. It is expected that more detailed papers analyzing both the model's simulation of the present day climate and its response to past and future changes in radiative forcing will follow.

Idealized radiative forcing scenarios, such as the 1% per year CO_2 increase examined here, have gained wide acceptance in the climate modeling community, in part because they facilitate intermodel comparisons and the analysis of modeled climate responses. For this reason, the 1% CO_2 increase to doubling protocol has been used successfully by the Coupled Model Intercomparison Project (CMIP). While not intended to specifically represent past or future trends in the real world's atmospheric composition, this rate of CO_2 increase produces a radiative forcing change that is similar to the Special Report on Emission Scenarios (SRES) A2 scenario (Nakicénović et al. 2002), which falls on the high side of the SRES scenarios. The straightforward approach of varying just one forcing agent (global atmospheric CO_2 levels) in a prescribed manner avoids ambiguities associated with more complicated and realistic scenarios. For example, by prescribing a 1% CO_2 increase to be the only forcing agent change, one does not need to consider intermodel differences in the spatial and temporal distributions of radiatively active aerosols—just one of the factors contained in more realistic forcing scenarios that can complicate and confound analyses and model intercomparisons. Of course, by adopting an idealized forcing scenario one loses the ability to directly compare the model results with historical observations. For this reason, most modeling groups conduct both idealized and more realistic forcing experiments. Results from CM2 experiments that used more complex forcing scenarios representing transient changes of several forcing agents over the past century and a half are presented in other papers, such as Part I.

2. Model description and experimental design

The CM2 coupled models and components are fully described in other papers (Parts I and II) and references therein. Only a brief description of the coupled model and its components is given here.

Two versions of the coupled model are developed, CM2.0 and CM2.1. The physical parameterizations and numerical algorithms used in the two versions are fairly similar; however, as shown in Part I, the climate drift of CM2.1 is quite smaller than that found in CM2.0. The descriptions below apply to both model versions unless noted otherwise. Only what we view as the major differences between CM2.0 and CM2.1 are found in the description below. The reader is again encouraged to seek additional details in the papers listed above.

The atmospheric component uses a horizontal grid spacing of 2° latitude by 2.5° longitude. There are 24 vertical levels. The CM2.0 atmospheric component uses a so-called "B grid" centered advection scheme in the horizontal. The CM2.1 atmospheric component uses the finite volume technique for its advection scheme (Lin 2004). The atmospheric physical parameterizations are described in detail in a paper by the GFDL Global Atmosphere Model Development Team (2004).

The ocean component is constructed from the Modular Ocean Model version 4 (MOM4) code (Griffies et al. 2003). A horizontal tripolar grid is used to avoid the North Pole singularity and the need for filtering in the Arctic Ocean. Everywhere south of 65°N grid points are separated by 1° of longitude. In the non-Arctic extratropics the north–south spacing is about 1° of latitude, but in the Tropics the spacing is reduced to a ⅓°

in the north–south direction. The ocean component uses 50 vertical levels, a bottom boundary layer parameterization, and partial grid cells at the bottom to more accurately represent bottom topography and its effect on the ocean's circulation. Unlike previous GFDL coupled models, CM2 uses explicit freshwater fluxes to simulate the exchange of water across the air–sea interface, rather than virtual salt fluxes (Griffies 2004).

One of the important differences between CM2.0 and CM2.1 is that CM2.1 uses a substantially smaller value for the oceanic viscosity in the extratropics. This results in a stronger subpolar gyre circulation in the North Atlantic, with associated stronger poleward heat transports and reduced sea ice in the North Atlantic, including the Labrador Sea. Oceanic convection is also enhanced in the Labrador Sea in CM2.1 relative to CM2.0, an important factor in understanding their differing responses to increasing greenhouse gases.

The land surface component has 18 vertical levels for heat storage, allowing for the simulation of the diurnal and seasonal cycles. Water storage uses a bucket, which mimics the root zone water availability and whose depth varies with soil and vegetation distributions. It has a second reservoir underneath the root zone that simulates groundwater storage. Evapotranspiration from the soil is limited by a nonwater-stressed stomatal resistance. Land cover types are prescribed. There is also a simple parameterization for frozen ground. A river routing scheme based upon the observed drainage maps is used to transport water to the ocean. The land component uses the same grid as the atmospheric component.

The CM2 sea ice component (Winton 2000) has full ice dynamics, three-layer thermodynamics (two ice, one snow), and a scheme for prognosing five different ice thickness categories and open water at each grid point. The sea ice model uses the same horizontal tripolar grid as the ocean component.

The component models pass fluxes across their interfaces using an exchange grid system (V. Balaji 2005, personal communication). The exchange grid enforces energy and mass conservation on the fluxes passed between the component models. The details of the coupling intervals and the differences in those intervals between CM2.0 and CM2.1 are found Part I.

To obtain the 1860 initial conditions for the CM2 coupled climate model's control integration, a method similar to that described by Stouffer et al. (2004) is used. In this method, the radiative conditions are set to 1860 and the model is allowed a few centuries to begin the adjustment to those conditions. Again, the reader is referred to Part I for the details of the methods used to obtain the 1860 control integrations. As mentioned above, the climate drift in the CM2.1 control integration is generally much smaller than that found in CM2.0.

The response of the coupled models to idealized radiative forcing changes is performed following the framework of the CMIP (Meehl et al. 2000) protocols. The coupled model is forced with a 1% per year (compounded) increase in atmospheric CO_2 concentration. Carbon dioxide doubling occurs at model year 70. After that point, the CO_2 concentration is held fixed at twice its normal value and the integrations continue for a total of 200 years. This integration is called the 1% integration. As noted by Manabe et al. (1991) and others, a 1% per year increase in the CO_2 concentration produces a nearly linear increase in the radiative forcing. The results from the CM2.0 and CM2.1 1% integrations are compared to their respective 1860 control integrations.

The time-dependent or transient response of the CM2 coupled models is compared to estimates of the equilibrium response obtained using SM2 atmosphere–slab or mixed layer ocean models. Two versions of the Slab Model version 2 (SM2) model are constructed, SM2.0 and SM2.1, corresponding to CM2.0 and CM2.1. Here the ocean components of the CM2 models are replaced by a slab ocean of uniform 50-m depth (Manabe and Stouffer 1980). These models allow no oceanic heat transport. The heat transports are accomplished through the use of heat flux adjustments (Hansen et al. 1984). By design, these models assume no changes in the ocean heat transport when the climate changes. They are a relatively inexpensive way (as compared to running the coupled model to equilibrium) to estimate the climate sensitivity of the coupled model to a doubling of the atmospheric CO_2 concentration. It needs to be noted that the term climate sensitivity in this paper has a specific definition: the equilibrium response of the globally averaged surface air temperature to a doubling of the atmospheric CO_2 concentration. Further details on the simulation and construction of the SM model are provided in T. Knutson et al. (2005, unpublished manuscript).

3. Results

a. Atmospheric changes

As the CO_2 concentration in the model atmosphere increases, the surface air temperature warms. In the 1% CM2.0 and CM2.1 integrations, the globally averaged surface air temperature warms by 1.6 and 1.5 K, respectively, by the time of CO_2 doubling (model year 70: Fig. 1 and Table 1). This value is called the transient climate

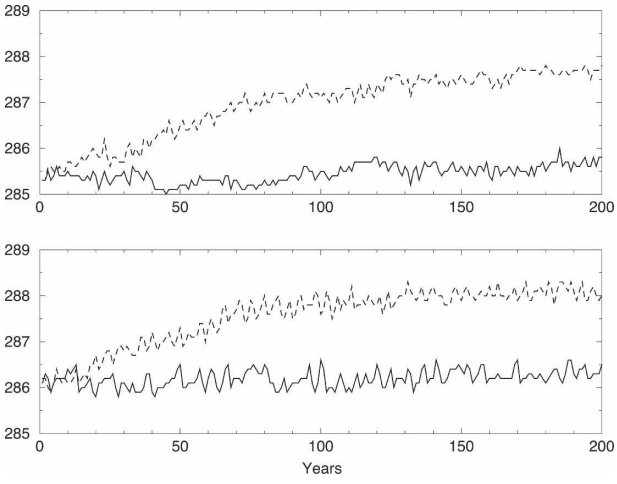

FIG. 1. Time series of global mean, annually averaged surface air temperature (K): (top) CM2.0 and (bottom) CM2.1 integrations. Solid line: 1860 control integrations; dashed line: 1% integrations.

response (TCR) (Cubasch et al. 2001). The TCR is defined as the globally averaged surface air temperature response in the 1% CO_2 increase integration (model years 61 to 80) minus the 100-yr time average from the control integration. The TCR obtained here lies just below the average TCR, 1.8 K, of all the global atmosphere–ocean general circulation models (AOGCMs) available at the time of the Working Group I 2001 Intergovernmental Panel on Climate Change (IPCC) Third Assessment Report (TAR) (Cubasch et al. 2001). However, the TCR obtained from both CM2 models lies well within the spread of results obtained from other models in the TAR.

TABLE 1. Values of climatically important variables. Definitions: Climate sensitivity and precipitation change are the globally averaged, equilibrium surface air temperature and precipitation difference ($2 \times CO_2$ minus control). The SM2 values represent annually averaged time averages over the last 50 years of the SM2 integrations. TCR is the transient climate response, which is the globally averaged surface air temperature difference. Precipitation change is the globally averaged percentage change in precipitation. THC change is the reduction of the maximum value of the overturning streamfunction in the North Atlantic Ocean. The TCR, precipitation, and THC changes for CM2 are computed over years 61–80 of the 1% integrations and years 1–100 of the 1860 control integrations.

	TCR (K)	Precipitation change (%)	THC change (Sv)
CM2.0	1.6	2.1	4
CM2.1	1.5	1.6	7
	Climate sensitivity (K)		
SM2.0	2.9	3.8	
SM2.1	3.4	4.9	

The TCR results from a blending of the climate sensitivity of the model and the amount of oceanic heat uptake during the transient integration. Loosely, one would expect that a model with a lower climate sensitivity would also have a lower TCR (Raper et al. 2002), the other important factor being the oceanic heat uptake.

The average climate sensitivity of the AOGCMs in the Cubasch et al. analysis is about 3 K with a TCR of about 1.8 K. The climate sensitivity of the older R15 and R30 GFDL models ranged from 3.4 to 3.7 K and their TCR is around 2 K (Dixon et al. 2003). The climate sensitivity of the CM2.0 and CM2.1 has been estimated to be 2.9 and 3.4 K, respectively (Table 1).

In the 1% CM2 integrations, the CO_2 concentration is held fixed after model year 70 at twice its normal value. The globally averaged surface air temperature continues to rise during the period when the CO_2 is not changing (Fig. 1). The temperature increases about 0.5 to 1 K in the 130-yr period after CO_2 doubling. The continued increase in globally averaged surface temperature points to the very long time scales of climate response found in the coupled system (Stouffer 2004).

The large-scale geographical distribution of the surface air temperature change taken around the time of CO_2 doubling is similar to what was found in earlier studies (Fig. 2) (e.g., Manabe et al. 1991; Washington and Meehl 1989). In both transient integrations, CM2.0 and CM2.1 (Figs. 2a and 2c), the warming is generally larger over the continents than the adjacent oceans and the warming is larger toward the North Pole. The warming is a minimum around Antarctica and in the northern North Atlantic Ocean. This pattern of warming is very similar to that shown in Cubasch et al. (2001, see their Fig. 10a). The magnitudes of the changes are somewhat smaller however, consistent with the smaller globally averaged warming noted above.

The minimum in the warming around Antarctica is more clearly seen in the zonally averaged surface air temperature response (Fig. 3). In both CM2 models, a minimum in the warming of about 0.6 K is located near 60°S. In CM2.1, this minimum is located a few degrees of latitude farther toward the south than in CM2.0. This shift is likely related to the difference in the locations of the wind stress maxima as discussed below. In the Tropics, the zonally averaged warming is about 1.5 K. It is a maximum in high latitudes of the Northern Hemisphere (about 3.5 K).

As expected, the equilibrium surface air temperature changes due to a doubling of the CO_2 concentration obtained from the atmosphere–slab ocean model

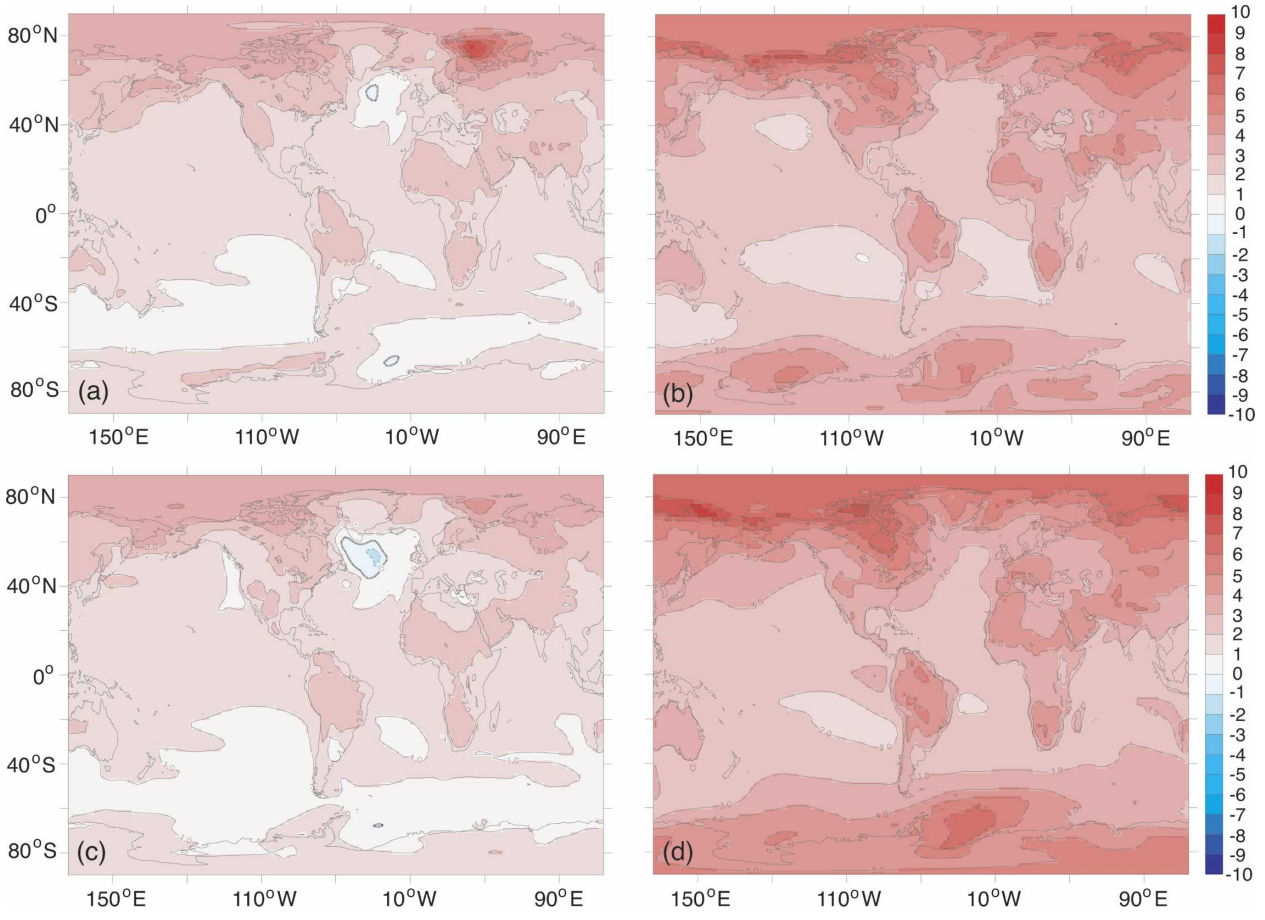

FIG. 2. Maps of annually averaged surface air temperature difference (K) for (a) the CM2.0 1% integration (model years 61–80) minus 1860 control integration (model years 1–100) and (b) the SM2.0 integration 2 × CO_2 minus control (50-yr time averages). (c) As in (a) but for CM2.1; (d) as in (b) but for SM2.1.

(SM2.0 and SM2.1: Figs. 2b and 2d) are larger than the transient changes (Figs. 2a and 2c). The temperature change patterns are also different in the coupled CM2 model integrations than in the atmosphere–slab ocean SM2 models. In the CM2 results, there is a region of very little temperature increase in the northern North Atlantic and in the Southern Ocean. These features are absent in the SM2 results, pointing to the large oceanic heat uptake in these regions. The large local warming in the Barents Sea region in the CM2.0 model (Fig. 2a) is also not seen in the equilibrium changes.

The difference in the surface air temperature response, CM2.0 to CM2.1, in the Barents Sea is related to differences in sea ice concentrations in the control simulations, leading to different sea ice responses in this region. The sea ice concentrations in the 1860 control integration are generally too large in CM2.0. As the model atmosphere warms in response to the increasing CO_2 in the atmosphere, the sea ice edge retreats (Fig. 4a). In the Barents Sea region, the retreating sea ice

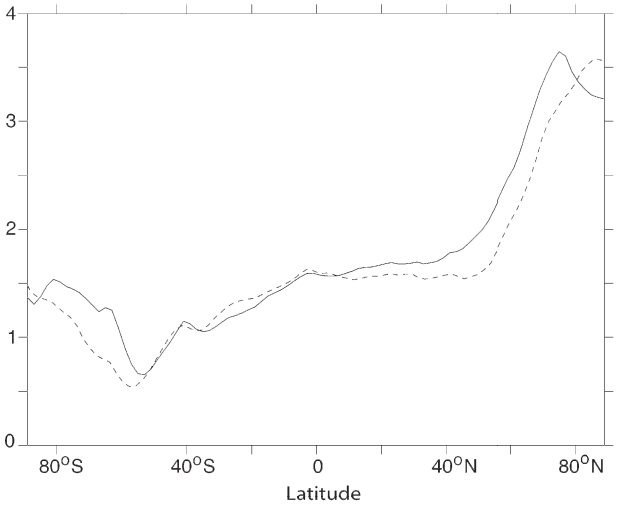

FIG. 3. Plot of annually averaged, zonally averaged surface air temperature difference (K), 1% integration (model years 61–80) minus 1860 control integration (model years 1–100). Solid line: CM2.0; dashed line: CM2.1.

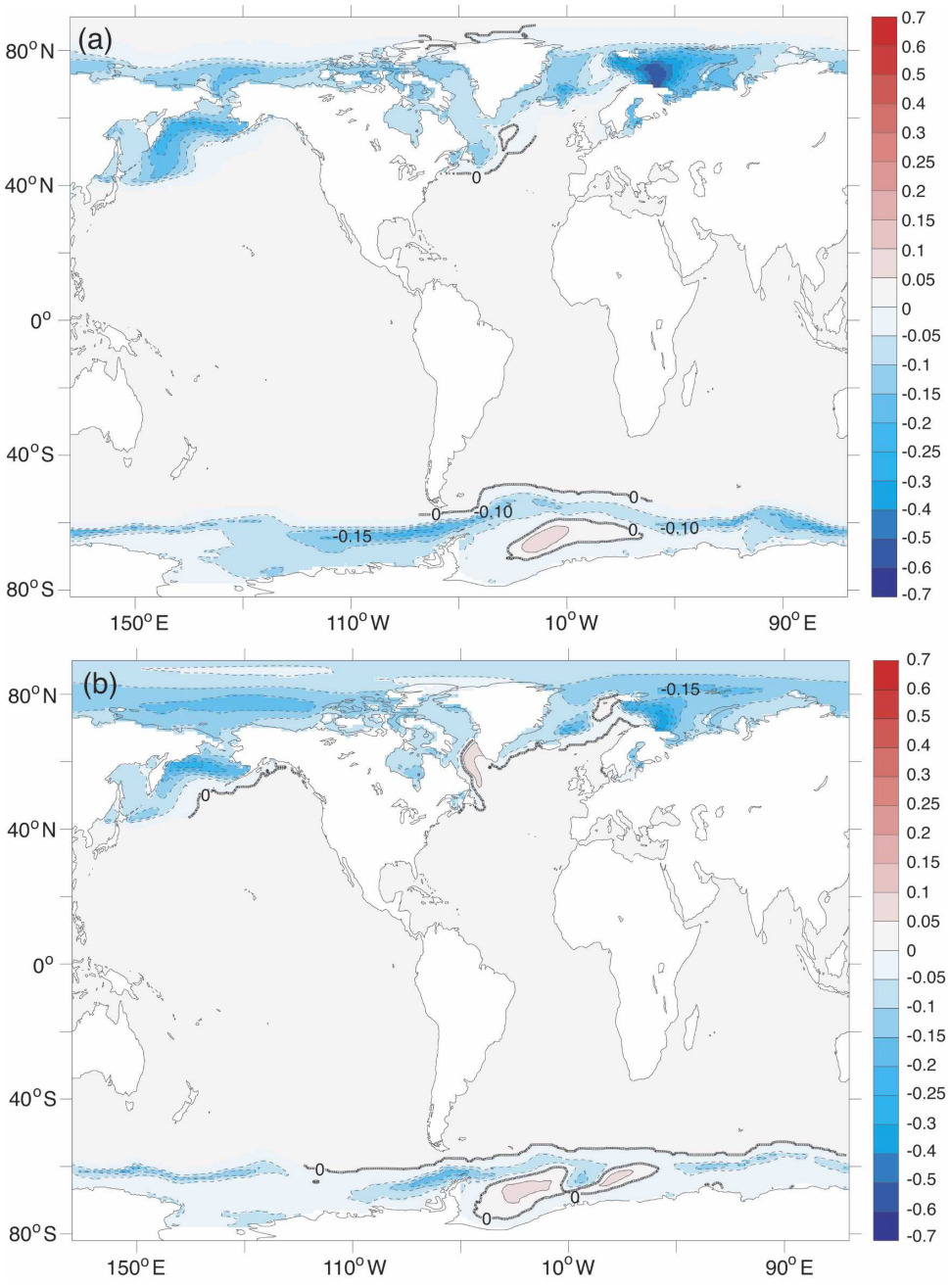

FIG. 4. Maps of annually averaged sea ice extent difference (fraction) for (a) CM2.0 and (b) CM2.1. The differences are constructed by subtracting the 1% integration (model years 61–80) minus 1860 control (model years 1–100). The contour interval is 0.05 (fraction) between −0.3 and 0.3; otherwise it is 0.1.

allows the atmosphere and ocean to more easily communicate with each other. This leads to deeper mixed layers and the formation of some deeper waters in this region in the CM2.0 integration. In the CM2.0 1% integration by the time of CO_2 doubling, the Barents Sea is ice free year-round. An ice-free Barents Sea with an associated increase in oceanic convection and an increase in the oceanic heat transport into this region results in the large local maximum in the warming.

In the CM2.1 1860 control, the sea ice concentrations are lower than in the CM2.0 1860 control. These differences lead to a smaller transient response in CM2.1 in

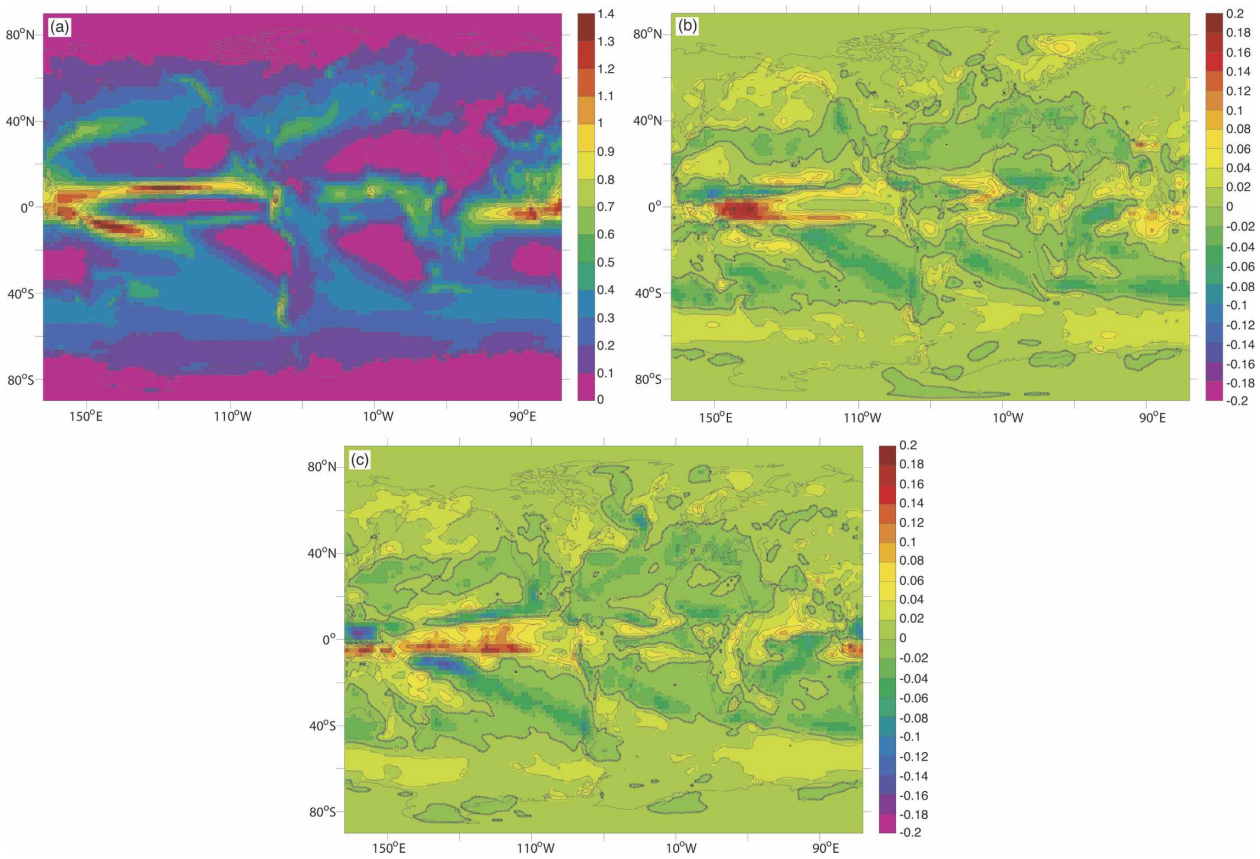

FIG. 5. Map of annually averaged precipitation rate (kg m^{-2} s^{-1}) for (a) the CM2.0 1860 control integration and (b) the CM2.0 difference and (c) CM2.1 difference. The differences are computed by subtracting the 1% integration (model years 61–80) minus 1860 control (model years 1–100). The time average for the control in (a) is computed over model years 1–100.

the Barents Sea region (Fig. 4b). A second area where CM2.1 sea ice changes differ from CM2.0 is in the western Arctic. Here the sea ice thicknesses in the CM2.1 1860 control are thinner than in CM2.0.

Sea ice changes in the Labrador Sea are also very different between the two model versions. In CM2.0, the ice retreats in the 1% integration (Fig. 4a). In CM2.1, there is more sea ice in the 1% integration than found in the control (Fig. 4b); that is, the sea ice is expanding in the CM2.1 1% integration. This sea ice change is associated with a reduction in the oceanic convection in the CM2.1 1% integration as compared to the control. The changes in the depth of the mixed layer in the Labrador Sea are shown in section 3b.

As the atmosphere warms, it can hold more water vapor and the hydrological cycle intensifies (Manabe et al. 1991). As a result, wet areas in the control climate tend to get wetter and dry areas tend to get drier. This generalization is seen in Fig. 5 by comparing the control simulation of precipitation to the change around the time of CO_2 doubling. Overall the control simulation (Fig. 5a) compares fairly well to observations. Model deficiencies included the presence of the so-called double ITCZ in the eastern tropical Pacific—a common model problem. Also, the Amazon basin is much too dry when compared to observations. Despite these problems, the major storm tracks and desert areas are clearly seen in the 1860 control simulation.

As CO_2 increases in the atmosphere, high latitudes of both hemispheres receive more precipitation (Figs. 5b and 5c). The precipitation in most of the tropical wet areas also increases. The precipitation tends to decrease in and near the subtropical dry areas, particularly in and around the continental deserts. This large-scale pattern of precipitation changes is very similar to that seen in earlier model studies (e.g., Manabe et al. 1991; Murphy and Mitchell 1995). By the time of CO_2 doubling, the global increase in the precipitation rate is about 2.1% in CM2.0 and 1.6% in CM2.1 (Table 1). As was the case for surface air temperature, this is close to the average model increase (2.5%) as found by Cubasch et al. (2001, see Fig. 9.3).

The equilibrium global precipitation increase in the SM2 models to a doubling of the CO_2 concentration is

3.8% in SM2.0 and 4.9% in SM2.1 (Table 1). The greater response in CM2.1 is likely related to its larger change in globally averaged surface air temperature: 3.4 K in CM2.1 and 2.9 K in CM2.0. The response in the fully coupled model, CM2, by the time of doubling is about half as large for both globally averaged surface air temperature and precipitation (Table 1).

In both model versions, the maximum in precipitation located over the Indonesian region moves eastward as the climate warms. In CM2.1 (Fig. 5c), the eastward movement is larger than in CM2.0 (Fig. 5b). As will be shown below, the warming in the eastern tropical Pacific is larger in CM2.1 than in CM2.0. The greater eastward shift of the precipitation maximum in CM2.1 is linked to the greater reduction of the tropical SST gradient in that model. The increased zonal asymmetry of the warming in the tropical Pacific, in turn, is likely tied to the stronger air–sea feedbacks through stronger tropical winds and weaker surface heat flux damping in CM2.1, which also contribute to a much stronger ENSO in that model compared to CM2.0 (Part III).

The atmospheric temperature change due to increasing CO_2 (Fig. 6) is very similar to earlier published results (e.g., Manabe et al. 1991; Cubasch et al. 2001, their Fig. 9.8). The warming is a maximum near the earth's surface in high latitudes of the Northern Hemisphere. This is due to the stability of the atmosphere, which traps the surface heating near the ground (Manabe and Stouffer 1979). The warming is also a maximum in the middle and upper troposphere in the Tropics. The stratosphere cools as CO_2 increases. The sign change between warming and cooling seen in the difference sections (Fig. 6) is located very close to the tropopause.

Atmospheric zonal wind changes by the time of CO_2 doubling are generally small, with the exception of the region near 40°S (Fig. 7). In this region, one notes a decrease in the zonal wind near 30°S and a region where it increased near 50°S. Comparing these latitudes to the placement of the zonal wind maximum in the 1860 control integrations (not shown) reveals that the Southern Hemisphere jet shifts southward and strengthens in both 1% integrations and that this shift extends through the whole troposphere. However, the latitude of the Southern Hemisphere jet in the 1860 control integrations is different in CM2.0 and CM2.1. In CM2.0, the jet is located equatorward of the observed placement by 3° or 4° of latitude. In CM2.1, the jet is very close to its observed location (Part I). In both model versions, the jet shifts poleward and strengthens in the Southern Hemisphere. The shift in the location of the Southern Hemisphere jet is associated with a trend toward the positive phase of the Southern Annular Mode (SAM). A similar jet shift and trend in the SAM has been noted by previous authors (e.g., Fyfe et al. 1999; Kushner et al. 2001).

In the Northern Hemisphere, there also seems to be a very weak tendency for a similar poleward shift in the zonally averaged zonal winds. However, the magnitude of the shift is very small. Further analysis of the zonal wind changes indicates that the zonal winds do shift toward the pole over the Atlantic Ocean sector with little or no shift in the Pacific Ocean sector. The trend in the Northern and Southern Hemisphere annular modes will be the subject of future investigations.

b. Ocean changes

This section describes changes that occur in the ocean model component around the time of CO_2 doubling in the atmosphere. The general pattern of the warming seen in the surface air temperature difference described above is also seen in the sea surface temperature (Fig. 8). The Tropics warm about 1.0 to 1.5 K by the time of CO_2 doubling in both model versions. The eastern tropical Pacific SSTs have a larger increase in CM2.1 than in CM2.0. The SSTs in the Barents Sea warm by more than 2 K in CM2.0 and by about 1.5 K in CM2.1. There is a large area of minimal warming around Antarctica and in the North Atlantic. In fact, there is a relatively large area of cooling in the North Atlantic in CM2.1. The cooling extends into the Labrador Sea in CM2.1. As discussed below, this is due to the very different climatic conditions in the control integrations of the two model versions.

As shown below, the general cooling in the North Atlantic is caused by a reduction in the poleward heat transport associated with a weakening of the thermohaline circulation (THC). There are also patches of relatively small warming seen in the subtropics, particularly in the Southern Hemisphere. These changes are associated with changes in the low-level winds and low clouds. Similar changes have been noted earlier in results obtained by other climate models (Gordon et al. 2000). The small changes in SST in the Arctic and near the Antarctic are due to the presence of sea ice in both the control and 1% integrations, keeping the SSTs near the freezing point of seawater.

As noted earlier, when the atmosphere warms, it can hold more water vapor and transports more water poleward. As a result, the high-latitude sea surface salinity (SSS) decreases (Fig. 9), particularly in the Northern Hemisphere. In the Tropics and subtropics, the changes are more mixed. In the eastern tropical Pacific and most of the tropical Atlantic, the increased evaporation associated with the atmospheric warming leads to the SSS

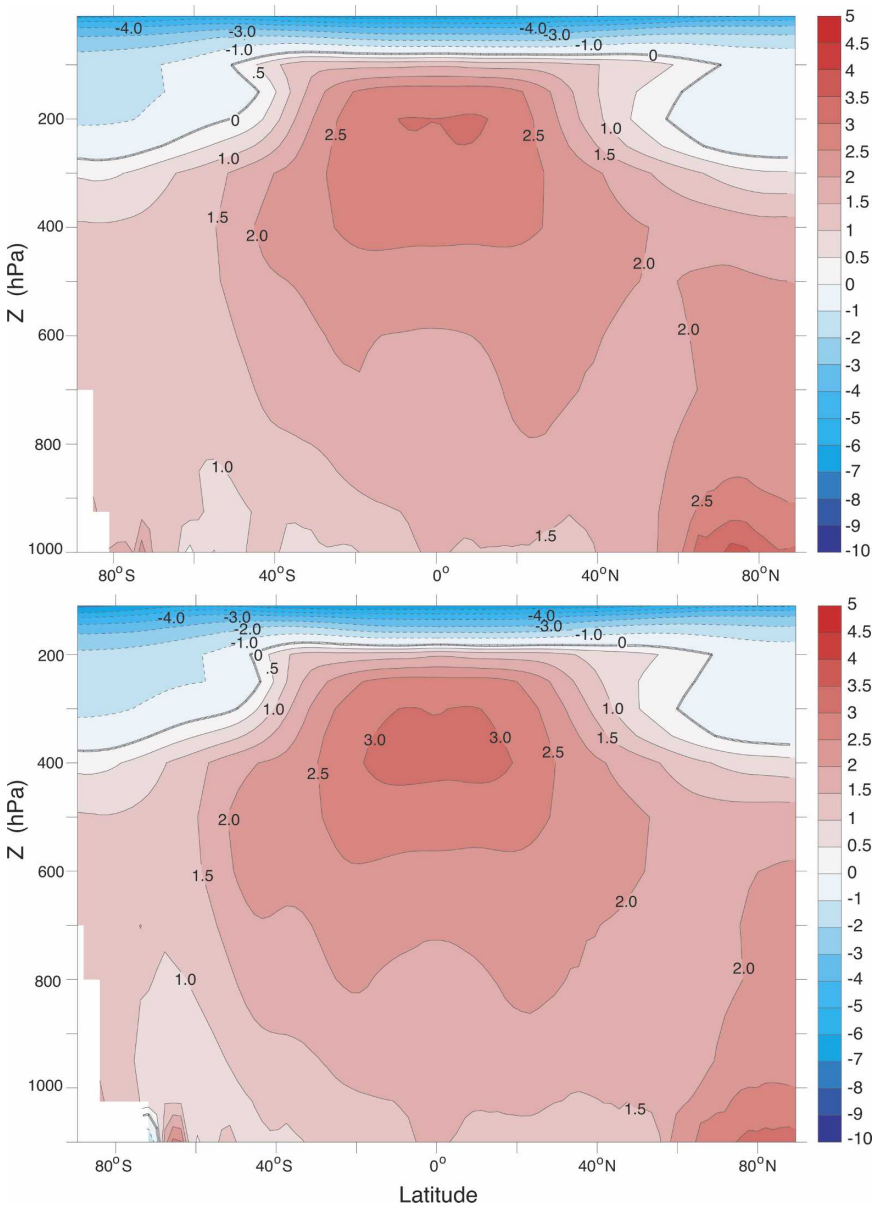

FIG. 6. Latitude–height sections of the zonally averaged, annually averaged atmospheric temperature differences (K) for (top) CM2.0 and (bottom) CM2.1. The difference is computed by subtracting the 1% integration (model years 61–80) minus 1860 control (model years 1–100). The contour interval is 1 K for negative values and 0.5 K for positive values.

generally increasing. In the western tropical Pacific, as noted above, there are relatively large precipitation increases, leading to the surface waters freshening in this region. The relatively large increases in sea surface salinity in the Atlantic from 40°N to 40°S are also likely associated with the reduction of the poleward salt transport and the longer residence times of the surface waters in an area where evaporation generally is greater than precipitation. The reduction of the northward salt transport and longer residence times are a result of the weakening of the THC as CO_2 increases in the model atmosphere as described below.

The weakening of the THC (Fig. 10) in response to increasing greenhouse gases has been found in earlier models (e.g., Manabe et al. 1991). The THC weakening is seen in most, but not all, AOGCMs (Cubasch et al. 2001). In CM2.0, the maximum value of the overturning streamfunction is about 18 Sv (1 Sv $\equiv 10^6$ m^3 s^{-1}) in the 1860 control integration. Around the time of CO_2 doubling in the model atmosphere, the THC weakens to

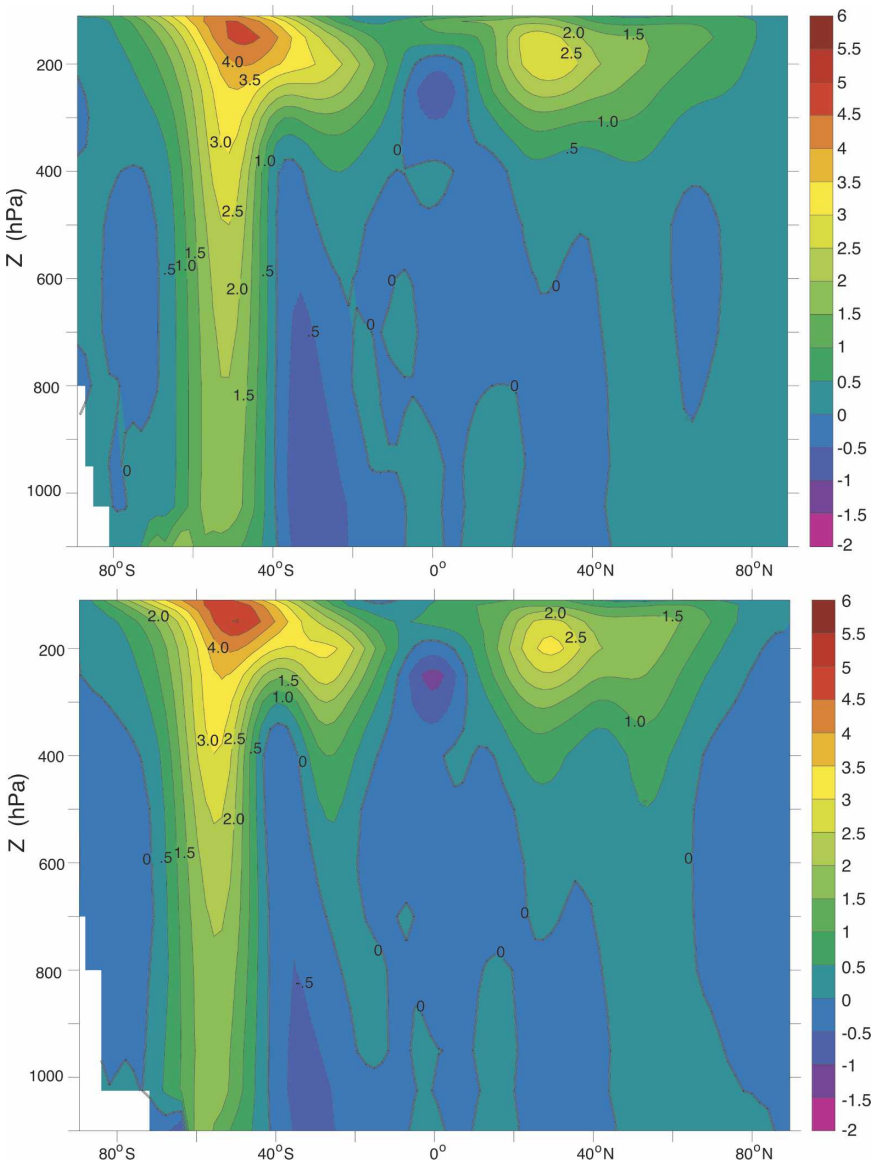

FIG. 7. As in Fig. 6 but for zonal wind (m s^{-1}).

about 14 Sv or about 18% (Table 1). This amount of weakening as a percentage of the control is fairly typical for recent AOGCMs (Cubasch et al. 2001).

The weakening of the THC is due to the increased vertical stability of the water column in high latitudes. As CO_2 increases, the ocean surface warms, increasing the vertical stability in most places. In high latitudes, the freshwater flux onto the ocean surface also increases (as discussed in section 3a). The increased freshwater flux lowers the surface salinity and, therefore, the density of the surface waters. This also leads to increased vertical stability of the water column, which inhibits deep convection and weakens the THC. Using the techniques of Dixon et al. (1999) and Gregory et al. (2005), experiments are underway to quantify the relative roles of the heat and freshwater surface flux changes in weakening the THC.

In the CM2.1 1860 control integration, the maximum value of the THC is about 24 Sv. In the course of our model development, we found that this increase in the CM2.1 1860 control THC strength is associated with the inclusion of the new atmospheric core in CM2.1 and changes in the oceanic viscosity, the latter being responsible for a major fraction of the increase (see model description section and Part II for more details). Around the time of CO_2 doubling in the CM2.1 1% integration, the THC weakens to about 17 Sv, a 29% reduction (Table 1). The reason for the larger THC

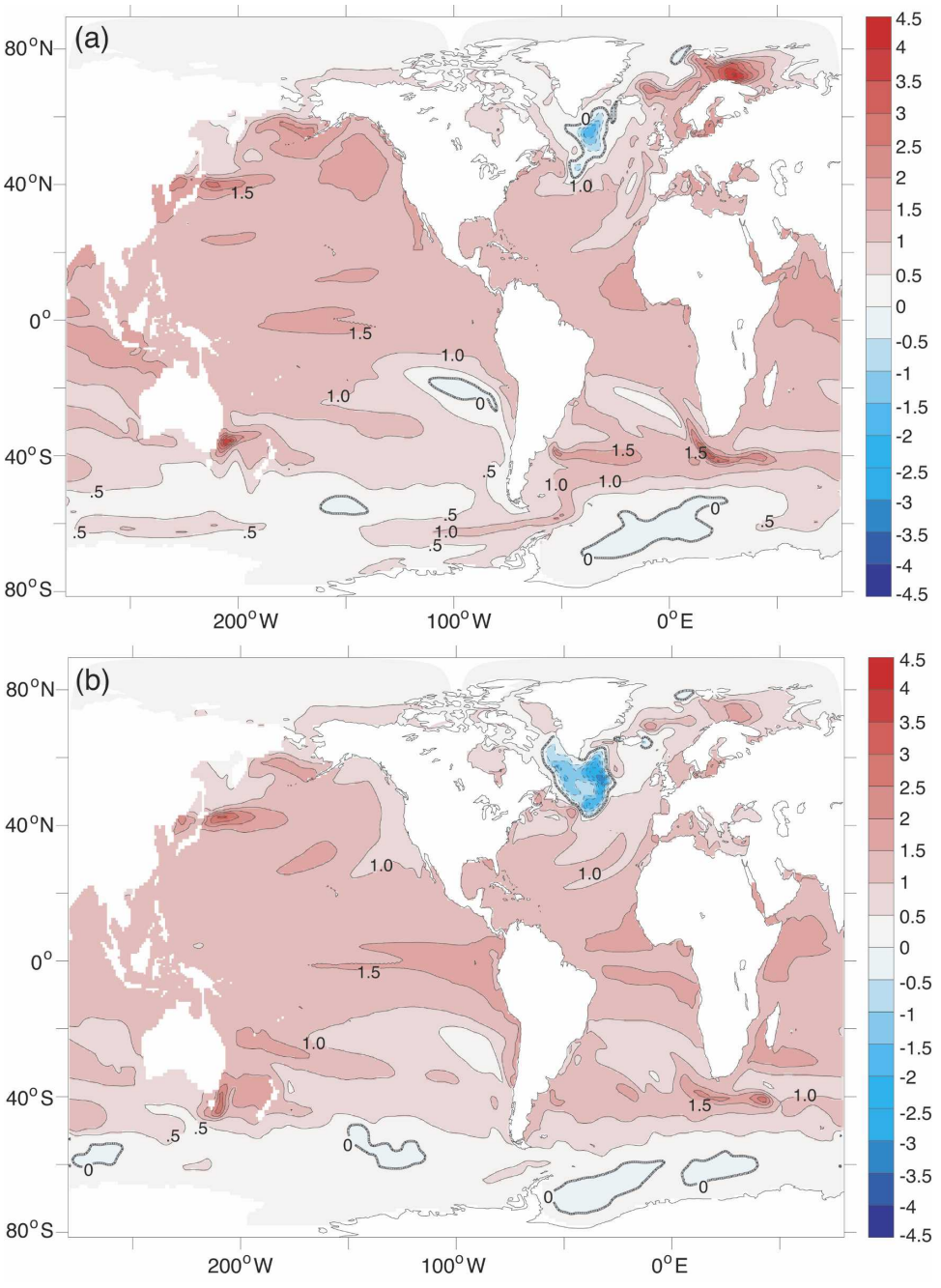

FIG. 8. Maps of annually averaged SST difference (K) for (a) CM2.0 and (b) CM2.1. The differences are constructed by subtracting the 1% integration (model years 61–80) minus 1860 control (model years 1–100).

reduction in the CM2.1 1% integration is not known but seems related to the large reduction of oceanic convection in the Labrador Sea, as discussed below.

After the CO_2 in the atmosphere stops increasing (model year 70), the THC begins a slow recovery toward its original strength. However, this recovery is not complete in either model by the end of the 1% integration (year 200). The slow recovery of the THC is also found in earlier model studies (e.g., Manabe and Stouffer 1994).

The weakening of the THC leads to a reduction in the northward heat transport (Fig. 11). In the 1860 control integration of both model versions, the maximum northward transport is found near 20°N and is about 2

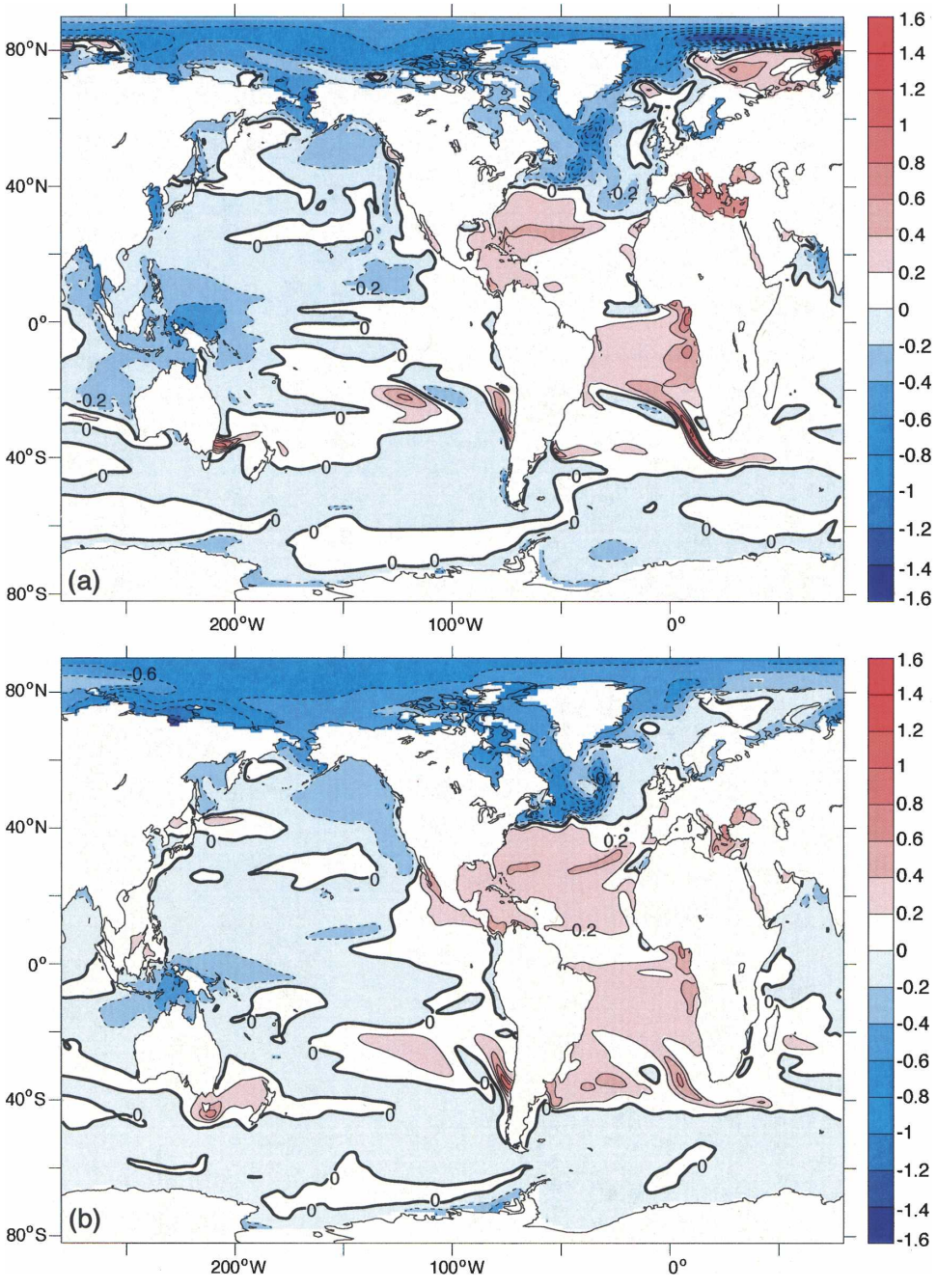

FIG. 9. As in Fig. 8 but for SSS difference (psu).

PW. Near 45°N, the northward heat transport is about 0.75 PW in both CM2 control integrations. In the 1% integration, these values reduce to about 1.8 PW at 20°N and 0.6 PW at 45°N. The reduction is slightly larger in CM2.1 than in CM2.0. The reduction in the northward heat transport leads to the minimum in the warming seen in the North Atlantic in the SST and surface air temperature maps. The larger reduction in northward heat transport in CM2.1 as compared with CM2.0 is consistent with the larger area of cooling seen in the northern North Atlantic SSTs in the CM2.1 (Fig. 8b).

Though SSTs increase over much of the globe, the warming penetrates deeper than 1000 m in only a few regions. These areas are places of deep- and intermediate-water formation in the model. In the CM2.0 Southern Hemisphere, there is a warming maximum of about 1 K located along the Antarctic continent and

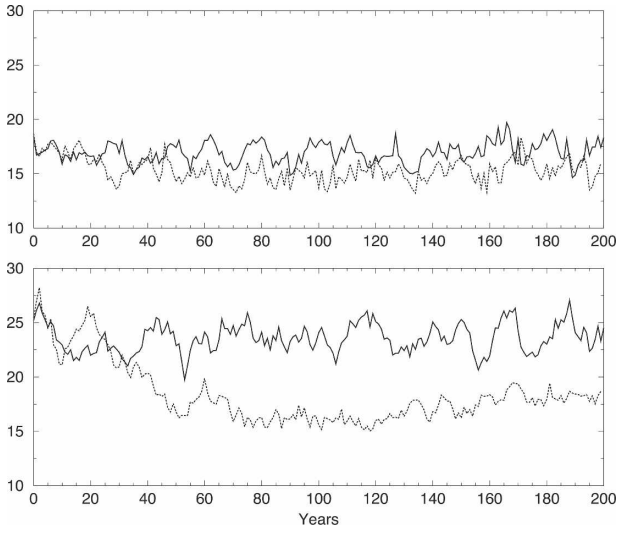

FIG. 10. Time series of the maximum value of the annually averaged overturning streamfunction (Sv) in the North Atlantic Ocean for (top) CM2.0 and (bottom) CM2.1. Solid line: 1860 control integration; dotted line: 1% integration.

800 m (Fig. 12a). This feature is absent or much smaller in CM2.1 (Fig. 12b). A second maximum, again about 1 K, is located near 400 m at 40°S in both model simulations. In the Northern Hemisphere of both model versions, the warming only penetrates to depth near 65° to 70°N, the Labrador and Greenland–Iceland–Norwegian (GIN) Seas. That the relatively large warming located near 500 m at this latitude lies over relative cooling near 2 km is evidence of capping by the SSS-driven decrease in surface density and is associated with the THC weakening (Manabe et al. 1991). The warming in CM2.1 near the surface in high northern latitudes is slightly smaller than in CM2.0. The cooling at depth is slightly larger in CM2.1. Again, this points to the greater reduction of the northward heat transport in CM2.1 as compared to CM2.0. At most other latitudes, there is very little penetration of the surface warming into deeper layers. The salinity section of the zonally averaged changes (not shown) indicates that the freshening of the high latitudes and increased salinity of the low-latitude surface layers also does not penetrate into the interior of the model ocean on these time scales.

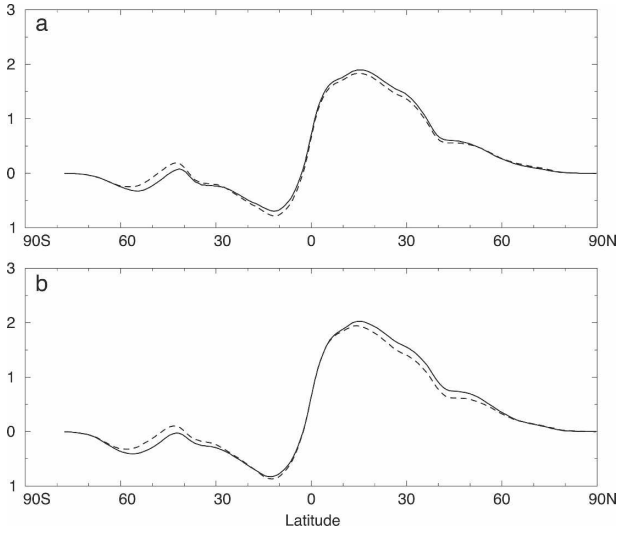

FIG. 11. Plot of zonally annually averaged oceanic northward heat transport (PW) for (a) CM2.0 and (b) CM2.1. Solid line: 1860 control integration (model years 1–100); dashed line: 1% integration (model years 61–80).

The differences in the oceanic heat uptake noted above contribute to the similarity of the TCR (globally averaged surface air temperature change at the time of doubling in an AOGCM forced by 1% per year CO_2 increase). As noted by Sarmiento et al. (1998), most of the oceanic heat uptake occurs in the Southern Ocean in response to increasing CO_2. The large differences in the penetration of the heat anomaly in the Northern Hemisphere between the two model simulations (Fig. 12), associated with changes in the model's THC (Fig. 10), do not result in large differences in the oceanic heat uptake owing to the relatively small area of the North Atlantic Ocean.

The zonally averaged zonal wind stress plot clearly shows the poleward shift of the Southern Hemisphere jet in the 1% integration (Fig. 13) in both model versions (discussed above) and is seen in earlier model results (Kushner et al. 2001). As noted earlier, the Southern Hemisphere jet maximum shifts poleward about 3° latitude in the 1% integrations. One also notes that the magnitude of the maximum value of the westerly stress increases as it shifts poleward in both model versions.

The poleward shift in the Southern Hemisphere winds in the CM2 1% integrations causes the Antarctic Circumpolar Current to move poleward. This shift is clearly evident in the sea surface height changes (Fig. 14). These sea surface height changes are only due to changes in the wind stress and sea ice weight on the ocean surface (they do not reflect changes due to ocean warming). In the Arctic and high latitudes, the large increases in sea surface height are due to the melting of sea ice. Melting sea ice both reduces the weight of the ice on the ocean surface and adds freshwater into the top ocean box, lowering the surface salinity and density. Both effects lead to increases in the sea surface height in the 1% integrations. In the CM2.1 sea surface height differences (Fig. 14b), there is an interesting pattern of changes in the North Atlantic Ocean. It is likely that

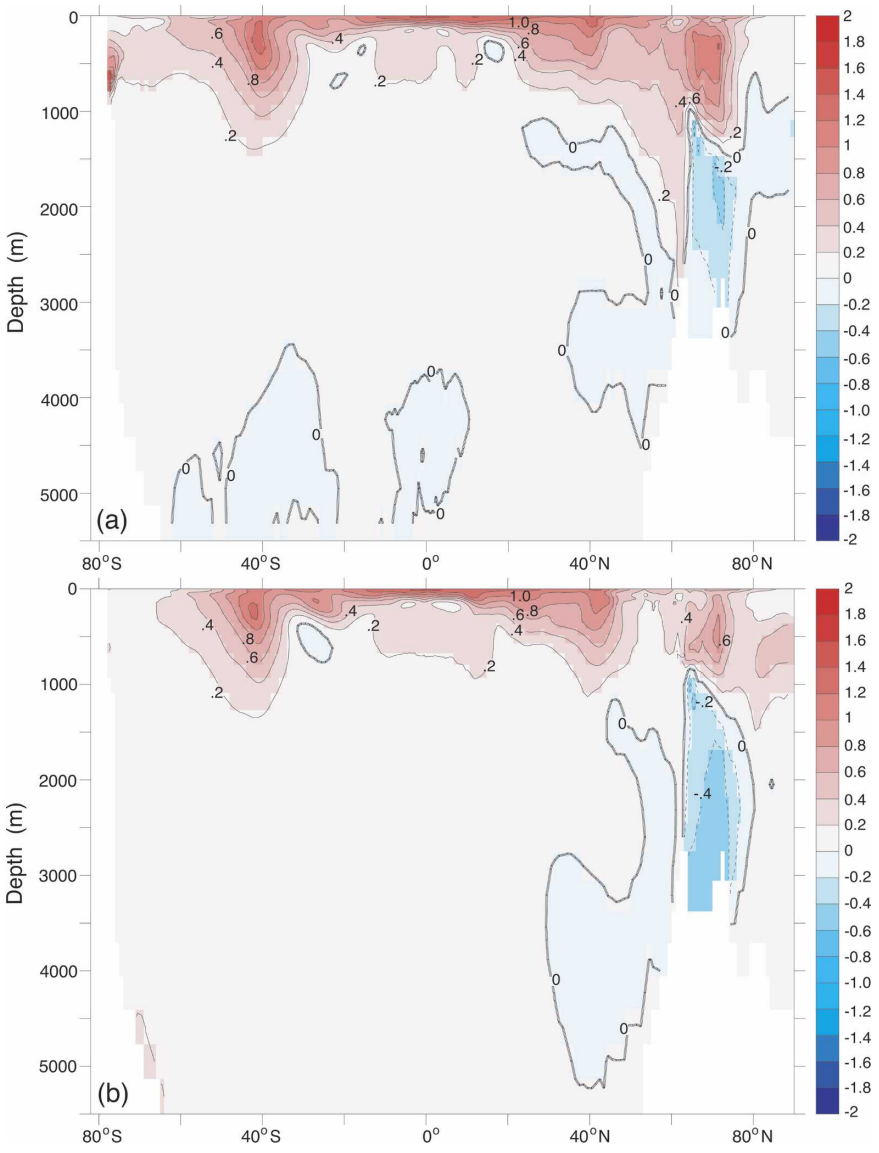

FIG. 12. Latitude–depth sections of the zonally annually averaged temperature differences (K), 1% integration (model years 61–80) minus 1860 control integration (model years 1–100), for (top) CM2.0 and (bottom) CM2.1.

these changes are related to changes in the oceanic convection in the Labrador Sea as discussed below.

In CM2.0 1860 control integrations, there is very little oceanic convection in the Labrador Sea so that the annually averaged mixed layer depths are less than 100 m as a long-term average (Fig. 15a) and are associated with the Labrador Sea being mainly ice covered in winter in CM2.0. In the CM2.1 1860 control integration, the annually averaged Labrador Sea mixed layer depths exceed 1 km (Fig. 15b) so that there is much less sea ice cover in the CM2.1 1860 control integration in the Labrador Sea when compared to CM2.0. The two simulations tend to fall well on either side of the observations of oceanic convection in the Labrador Sea (Part II). The causes for this difference in the simulation of the Labrador Sea mixed layer depths are unclear. However, at least one important factor is the increased heat transport into this region in the CM2.1 results as noted above. This allows the waters of the Labrador Sea to be sea ice free for more of the annual cycle, allowing interactions between the atmospheric buoyancy fluxes and the oceanic convection.

As the climate warms in response to the increasing CO_2 in the atmosphere, the response in the Labrador region is very different between the two model versions. In CM2.0, the extensive sea ice coverage retreats,

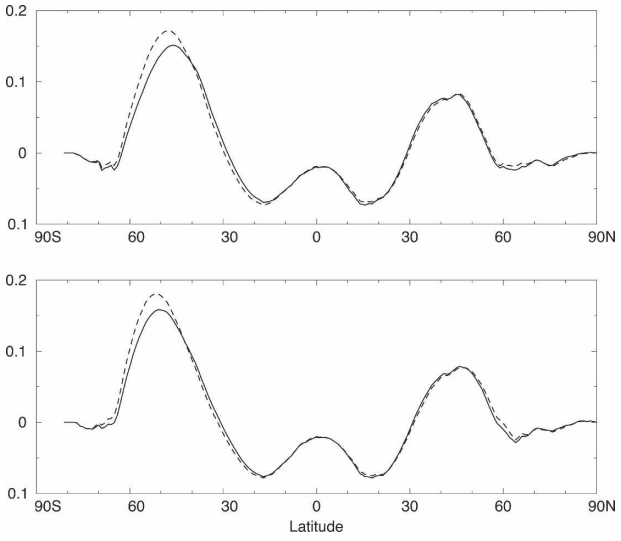

FIG. 13. Plots of the zonally annually averaged wind stress ($m^2\ s^{-1}$) for (top) CM2.0 and (bottom) CM2.1. Solid line: 1860 control integration (model years 1–100); dashed line: 1% integration.

resulting in less sea ice coverage in the CM2.0 1% integration (Fig. 4a). This climate change hardly affects the mixed layer depth (Fig. 15c). In CM2.1, the oceanic convection greatly decreases, resulting in much shallower mixed layers (Fig. 15d). The reduction of oceanic convection is associated with more sea ice formation in winter, resulting in a small increase in the sea ice coverage (Fig. 4b). It is likely that the reduction in the oceanic convection in CM2.1 in the Labrador Sea leads to the larger reduction in the THC and associated northward heat transport. This is an interesting case where differences in the control climate simulation lead to very different responses in the perturbed climate.

The differences in the Labrador Sea climate response in the two models are mainly confined to the local region. As documented in the rest of the paper, the response of the two models is very similar.

Over the rest of the North Atlantic region, the mixed layer generally shoals in both model versions by the time of CO_2 doubling (Fig. 15). This is due to the surface waters becoming lighter, either through warming or freshening (or both), depending on location. The lighter surface waters hinder the mixing of the surface waters to depth. This results in less oceanic convection and mixing, leading to the reduction of the THC in both model versions.

The collapse of the Labrador Sea convection noted here in the CM2.1 model version is very similar to that reported in Wood et al. (1999) in the Third Hadley Centre Coupled Ocean–Atmosphere GCM (HadCM3) model. In both models, the oceanic convection in the Labrador Sea shuts down or is greatly reduced as the CO_2 concentration increases in the model atmosphere. As noted above, this is not the case in CM2.0, where there is little or no Labrador Sea convection in the 1860 control integration.

4. Summary

Results obtained from two new versions of the GFDL CM2 coupled climate model are presented. We have documented both the coupled model's response to an increase of CO_2 at the rate of 1% per year until doubling (following the CMIP protocol) as well as the response to an instantaneous doubling of CO_2 of the atmosphere model coupled to a slab ocean model. These new CM2 models are very different from earlier GFDL global coupled model versions in their parameterizations of subgrid-scale physical processes, numerical algorithms, and increased resolution. Unlike previous versions of the GFDL climate model, CM2 does not use flux adjustment to maintain a stable control climate. The models are constructed to be useful for a wide range of applications, from seasonal-to-interannual predictions to multicentennial climate change research.

The thermohaline circulation response to increasing atmospheric CO_2 in CM2.1 is slightly larger than that found in CM2.0. However, the THC in the CM2.1 1860 control integration is also larger than in CM2.0. The sea ice response in the Labrador Sea is very different in the two model versions. In the CM2.0 1860 control integration, there is very little oceanic convection and extensive sea ice cover. In the 1% CM2.0 integration, some of this sea ice melts, resulting in less sea ice cover. In contrast, in the CM2.1 1860 control integration, there is very active oceanic convection and only a relatively small amount of sea ice coverage. In the CM2.1 1% integration, the oceanic convection is reduced and the sea ice coverage increases. These differences in response point to the importance of the control climate. In spite of the differences in the climate response in the Labrador Sea region, the overall climate response to increasing CO_2 is quite similar in the two CM2 models, particularly in the patterns of the response.

A new feature of the CM2 climate model is the use of a true freshwater flux boundary condition in the formulation of the ocean model. All earlier ocean component models convert the freshwater flux into a virtual salt flux to change the ocean's surface salinity. Here, the freshwater flux changes the volume of the top ocean grid box, producing a more accurate change in the surface salinity in response to the surface fluxes (Griffies et al. 2005). In the past, the virtual salt flux was viewed

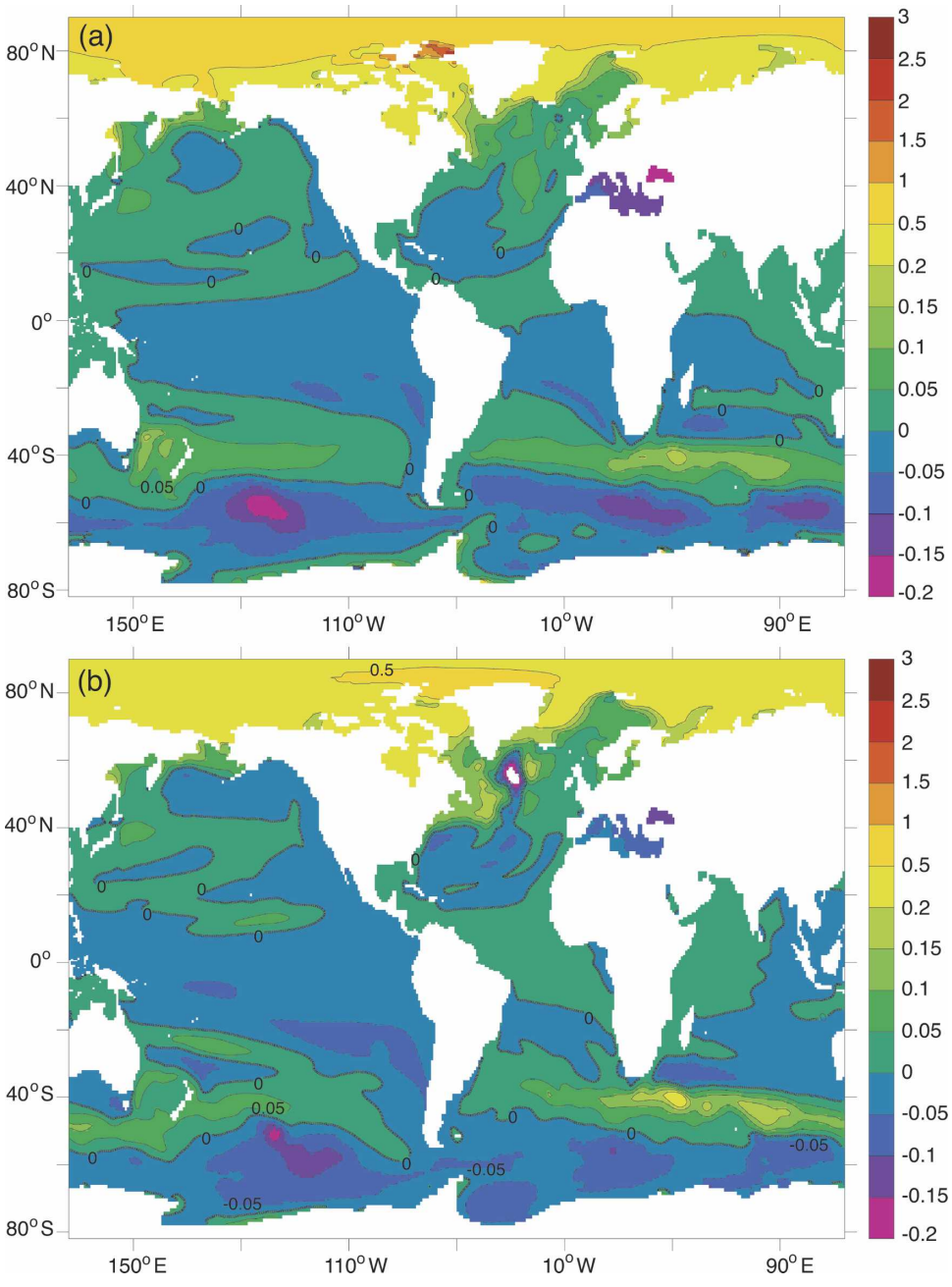

FIG. 14. Maps of the annually averaged sea surface height difference (m), 1% integration (model years 61–80) minus 1860 control integration (model years 1–100), for (a) CM2.0 and (b) CM2.1.

as a reason for concern and uncertainty in the projections obtained from climate models. Since the response of this model is grossly similar to earlier models, it appears that the use of virtual salt flux boundary conditions is not a major problem. Plans have been developed to quantify the differences in the model's response to a freshwater perturbation using the virtual salt flux technique and the realistic water fluxes in the model presented here.

The surface air temperature climate sensitivity is 2.9 (SM2.0) and 3.4 K (SM2.1) for a doubling of the atmosphere CO_2 concentration as estimated by an atmosphere–slab ocean model. The transient climate response (TCR) around the time of CO_2 doubling found in the coupled model when forced by a 1% CO_2 increase is about 1.6 K for both model versions (CM2.0 and CM2.1). In response to a doubling of the CO_2 concentration, the globally averaged precipitation in-

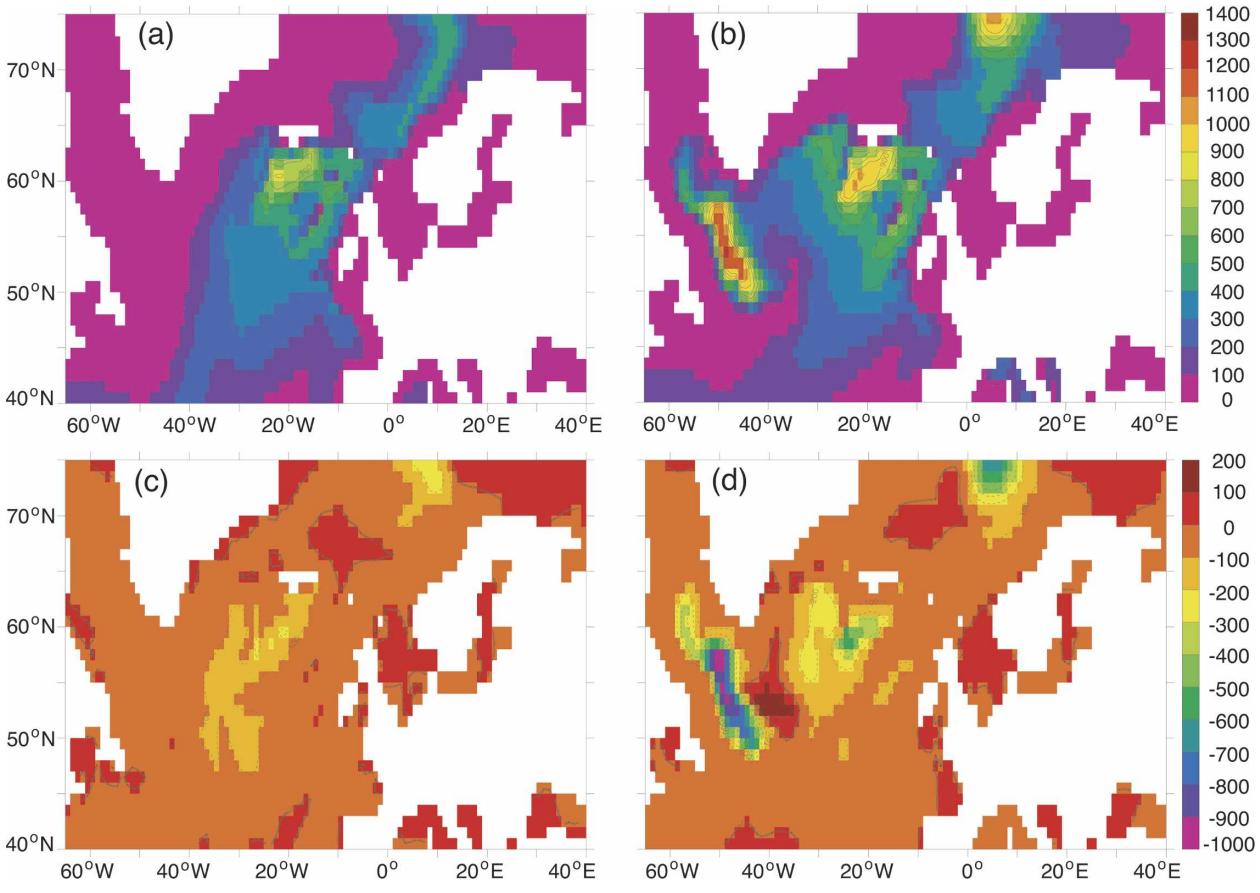

FIG. 15. Maps of annually averaged mixed layer depth (m) for (a), (b) 1860 control integration and (c), (d) difference 1% integration (model years 61–80) minus 1860 control integration (model years 1–100). (a), (c) CM2.0 and (b), (d) CM2.1. The mixed layer is defined as the depth where the buoyancy difference with respect to the surface level is greater than or equal to 0.0003 m s^{-2}.

creases by 3.8% in SM2.0 and 4.9% in SM2.1. By the time of CO_2 doubling in the coupled model, these increases were 2.1% (CM2.0) and 1.6% (CM2.1). The surface air temperature and the precipitation responses suggest that these new GFDL model versions are very close to the average model response seen in Cubasch et al. (2001).

Acknowledgments. We wish to thank Ants Leetmaa and Jerry Mahlman (present and past GFDL directors) for their support in building and running these models. We also thank R. Toggweiler, H. Levy II, and two anonymous reviewers for their helpful comments on earlier versions of this manuscript.

REFERENCES

Cubasch, U., and Coauthors, 2001: Projections of future climate change. *Climate Change 2001: The Scientific Basis,* J. T. Houghton et al., Eds., Cambridge University Press, 526–582.

Delworth, T. L., R. J. Stouffer, K. W. Dixon, M. J. Spelman, T. R. Knutson, A. J. Broccoli, P. J. Kushner, and R. T. Wetherald, 2002: Review of simulations of climate variability and change with the GFDL R30 coupled climate model. *Climate Dyn.,* **19,** 555–574.

——, and Coauthors, 2006: GFDL's CM2 global coupled climate models. Part I: Formulation and simulation characteristics. *J. Climate,* **19,** 643–674.

Dixon, K. W., T. L. Delworth, M. J. Spelman, and R. J. Stouffer, 1999: The influence of transient surface fluxes on North Atlantic overturning in a coupled GCM climate change experiment. *Geophys. Res. Lett.,* **26,** 2749–2752.

——, ——, T. R. Knutson, M. J. Spelman, and R. J. Stouffer, 2003: A comparison of climate change simulations produced by two GFDL coupled climate models. *Global Planet. Change,* **37,** 81–102.

Fyfe, J. C., G. J. Boer, and G. M. Flato, 1999: The Arctic and Antarctic Oscillations and their projected changes under global warming. *Geophys. Res. Lett.,* **26,** 1601–1604.

GFDL Global Atmospheric Model Development Team, 2004: The new GFDL global atmosphere and land model AM2–LM2: Evaluation with prescribed SST simulations. *J. Climate,* **17,** 4641–4673.

Gnanadesikan, A., and Coauthors, 2006: GFDL's CM2 global coupled climate models. Part II: The baseline ocean simulation. *J. Climate,* **19,** 675–697.

Gordon, C., C. Cooper, C. A. Senior, H. Banks, J. M. Gregory, T. C. Johns, J. F. B. Mitchell, and R. A. Wood, 2000: The simulation of SST, sea ice extents and ocean heat transport in a version of the Hadley Centre coupled model without flux adjustments. *Climate Dyn.,* **16,** 147–168.

Gregory, J. M., and Coauthors, 2005: A model intercomparison of changes in the Atlantic thermohaline circulation in response to increasing atmospheric CO_2 concentration. *Geophys. Res. Lett.,* **32,** L12703, doi:10.1029/2005GL023209.

Griffies, S. M., 2004: *Fundamentals of Ocean Models*. Princeton University Press, 496 pp.

——, M. J. Harrison, R. C. Pacanowski, and A. Rosati, 2003: A technical guide to MOM4. GFDL Ocean Group Tech. Rep. 5, NOAA/Geophysical Fluid Dynamics Laboratory, Princeton, NJ, 295 pp.

——, and Coauthors, 2005: Formulation of an ocean model for global climate simulations. *Ocean Sci.,* **1,** 45–79.

Hansen, J., A. Lacis, D. Rind, G. Russell, P. Stone, I. Fung, R. Ruedy, and J. Lerner, 1984: Climate sensitivity: Analysis of feedback mechanisms. *Climate Processes and Climate Sensitivity*, J. E. Hansen and T. Takahashi, Eds., Amer. Geophys. Union, 130–163.

Kushner, P. J., I. M. Held, and T. L. Delworth, 2001: Southern Hemisphere atmospheric circulation response to global warming. *J. Climate,* **14,** 2238–2249.

Lin, S. J., 2004: A "vertically Lagranian" finite-volume dynamical core for global models. *Mon. Wea. Rev.,* **132**, 2293–2307.

Manabe, S., and R. J. Stouffer, 1979: A CO_2 climate sensitivity study with a mathematical model of the global climate. *Nature,* **282,** 491–493.

——, and ——, 1980: Sensitivity of a global climate model to an increase of CO_2 concentration in the atmosphere. *J. Geophys. Res.,* **85** (C10), 5529–5554.

——, and ——, 1988: Two stable equilibria of a coupled ocean–atmosphere model. *J. Climate,* **1,** 841–866.

——, and ——, 1994: Multiple-century response of a coupled ocean–atmosphere model to an increase of atmospheric carbon dioxide. *J. Climate,* **7,** 5–23.

——, ——, M. J. Spelman, and K. Bryan, 1991: Transient responses of a coupled ocean–atmosphere model to gradual changes of atmospheric CO_2. Part I: Annual mean response. *J. Climate,* **4,** 785–818.

Meehl, G. A., G. J. Boer, C. Covey, M. Latif, and R. J. Stouffer, 2000: The Coupled Model Intercomparison Project (CMIP). *Bull. Amer. Meteor. Soc.,* **81,** 313–318.

Murphy, J. M., and J. F. B. Mitchell, 1995: Transient response of the Hadley Centre coupled ocean–atmosphere model to increasing carbon dioxide. Part II: Spatial and temporal structure of response. *J. Climate,* **8,** 57–80.

Nakićenović, N. J., and Coauthors, 2000: *IPCC Special Report on Emission Scenarios*. Cambridge University Press, 599 pp.

Raper, S. C. B., J. M. Gregory, and R. J. Stouffer, 2002: The role of climate sensitivity and ocean heat uptake on AOGCM transient temperature response. *J. Climate,* **15,** 124–130.

Rosati, A., K. Miyakoda, and R. Gudgel, 1997: The impact of ocean initial conditions on ENSO forecasting with a coupled model. *Mon. Wea. Rev.,* **125,** 754–772.

Sarmiento, J. L., T. M. C. Hughes, R. J. Stouffer, and S. Manabe, 1998: Simulated response of the ocean carbon cycle to anthropogenic climate warming. *Nature,* **393,** 245–249.

Sausen, R., K. Barthel, and K. Hasselmann, 1988: Coupled ocean-atmosphere models with flux corrections. *Climate Dyn.,* **2,** 154–163.

Stouffer, R. J., 2004: Time scales of climate response. *J. Climate,* **17,** 209–217.

——, A. J. Weaver, and M. Eby, 2004: A method for obtaining pre-twentieth century initial conditions for use in climate change studies. *Climate Dyn.,* **23,** 327–339.

Washington, W. M., and G. A. Meehl, 1989: Climate sensitivity due to increased CO_2: Experiments with a coupled atmosphere and ocean general circulation model. *Climate Dyn.,* **4,** 1–38.

Winton, M., 2000: A reformulated three-layer sea ice model. *J. Atmos. Oceanic Technol.,* **17,** 525–531.

Wittenberg, A. T., A. Rosati, N.-C. Lau, and J. J. Ploshay, 2006: GFDL's CM2 global coupled climate models. Part III: Tropical Pacific climate and ENSO. *J. Climate,* **19,** 698–722.

Wood, R. A., A. B. Keen, J. F. B. Mitchell, and J. M. Gregory, 1999: Changing spatial structure of the thermohaline circulation in response to atmospheric CO_2 forcing in a climate model. *Nature,* **399,** 572–575.